

## Article

# Frequency-Reconfigurable Microstrip Patch Antenna Based on Graphene Film

Xinhai Wang<sup>1,2</sup>, Liqiong Wu<sup>3</sup>, Hua Chen<sup>1</sup> , Wei Wang<sup>2,\*</sup> and Zhaoping Liu<sup>2,3,\*</sup>

<sup>1</sup> Faculty of Electrical Engineering and Computer Science, Ningbo University, Ningbo 315211, China; dkchenhua0714@hotmail.com (H.C.)

<sup>2</sup> Key Laboratory of Graphene Technologies and Applications of Zhejiang Province, CAS Engineering Laboratory for Graphene, Ningbo Institute of Materials Technology & Engineering, Chinese Academy of Sciences, Ningbo 315201, China

<sup>3</sup> National Graphene Manufacturing Innovation Center, Ningbo 315201, China

\* Correspondence: wangwei@nimte.ac.cn (W.W.); liuzp@nimte.ac.cn (Z.L.)

**Abstract:** Fifth-generation mobile communication systems must connect to multiple wireless networks. In order to enable a single device to match the frequency bands of multiple wireless networks, it is usually necessary to use multiple single-band or multi-band antennas, which occupy a large amount of space inside a given device. Using frequency-reconfigurable antennas to replace multiple single-function antennas is an effective way to solve this problem. In this paper, we propose a frequency-reconfigurable microstrip patch antenna based on graphene film, which fills the slot of the radiating patch with graphene film. It was found that the surface current of the antenna can be changed by changing the conductivity of graphene through bias voltage, which allows the operating mode of the antenna to switch between a nearly slotted antenna and a nearly unslotted antenna to achieve frequency reconfigurability. By changing the bias voltage from 0 V to 9 V, the resonant frequency of the antenna can be switched from 29.6 GHz to 40 GHz, and the center frequency can be altered by 10.4 GHz, corresponding to the reflection coefficients of  $-26$  dB and  $-20.8$  dB, respectively. The antenna achieves good matching in both operating modes.

**Keywords:** frequency-reconfigurable antenna; graphene; tunable conductivity; voltage control



**Citation:** Wang, X.; Wu, L.; Chen, H.; Wang, W.; Liu, Z.

Frequency-Reconfigurable Microstrip Patch Antenna Based on Graphene Film. *Electronics* **2023**, *12*, 2307. <https://doi.org/10.3390/electronics12102307>

Academic Editor: Dal Ahn

Received: 13 April 2023

Revised: 10 May 2023

Accepted: 18 May 2023

Published: 19 May 2023



**Copyright:** © 2023 by the authors. Licensee MDPI, Basel, Switzerland. This article is an open access article distributed under the terms and conditions of the Creative Commons Attribution (CC BY) license (<https://creativecommons.org/licenses/by/4.0/>).

## 1. Introduction

Fifth-generation (5G) mobile communication systems, constituting the main direction of next-generation mobile communication technology, features high speed, low latency, and wide connectivity [1]. 5G communication devices must be equipped with many single-band or multi-band antennas in order to comply with multiple wireless networks, thereby filling the limited space available in the device [2]. Reconfigurable antennas can be used to achieve multiple objectives with one antenna instead of two or more antennas [3]. Frequency-reconfigurable antennas utilize the same antenna to meet the required multiple communication bands and do not use multiple antennas operating at different frequencies for signal transmission or reception, which not only saves space and cost but also improves the performance of a device [4–6]. Therefore, the use of reconfigurable antennas instead of single-function antennas is an effective approach to solving such problems.

In 1979, “reconfigurability” was defined as “the ability to adjust the beam shape on command” [7]. Four main types of techniques are generally used to achieve reconfigurable antennas: switching structures, mechanically movable components, antenna arrays, and variable materials [8]. The most commonly used switching structures are electronically controlled switching structures such as PIN (positive-intrinsic-negative) diodes [9,10], variable capacitors [11], and radio frequency microelectromechanical system (RF-MEMS) switches [12,13]. However, RF-MEMS switches are costly [14], PIN diodes affect overall

system performance [15] and have mechanical movable parts [16–18], and array antennas [19,20] are hindered by their large size. So, new methods of developing reconfigurable antennas still need to be developed. Graphene was first prepared in a laboratory in 2004 [21] and has since been employed in various applications to improve the performance of devices due to its excellent properties such as good electrical conductivity and high mechanical strength [22–26]. In addition, graphene is also attractive in the field of reconfigurable antennas because of its tunable conductivity [27–31].

In 2008, Hanson performed a theoretical analysis of the electrical conductivity of graphene and concluded that the conductivity of graphene changed with the application of a biased electric or biased magnetic field [32]. This property of graphene allows it to be employed as a theoretical basis for reconfigurable antennas. As early as 2012, Julien Perruisseau-Carrier's team had applied graphene in the field of frequency-reconfigurable antennas. They applied graphene to a microstrip patch antenna in the terahertz band, replacing the patch of the antenna with graphene while retaining the metallic composition of the microstrip line, and investigated the antenna's performance [33]. The results of the study indicated that the resonant frequencies of the antenna corresponded to 12 THz, 17 THz, and 21 THz for graphene chemical potentials of 0.25 eV, 0.5 eV, and 0.75 eV, respectively. The resonant frequency of the antenna increased with the increase in the graphene chemical potential, presenting an approximately linear increase.

In 2015, Dragoman's team designed and tested a microwave slot antenna based on a graphene coplanar structure. They transferred graphene grown via the chemical vapor deposition (CVD) method to a silicon wafer and combined it with a metal coplanar surface to fabricate the antenna [34]. Consequently, the reflection coefficient changed, and a 24 MHz shift in the center frequency was achieved after imposing the bias voltage. In addition, the radiation efficiency of the graphene antenna was lower than that of the metal antenna, but the bandwidth of the graphene antenna was much larger than that of the metal antenna with the same geometry and operating frequency. In the same year, the research team also designed a slit antenna operating in the X-band [35], where a square graphene film was loaded in the upper slit and the reflection coefficient of the antenna was modulated by applying a bias voltage of  $-20-0$  V to the graphene film, which altered the reflection coefficient by 20 dB, although the center frequency was only shifted by 7.5 MHz.

In 2017, Yasir et al. attached a graphene film to the short stub above a patch antenna, and the access state of the short stub was changed by applying bias voltage to change the antenna's input impedance, thus shifting the center frequency of the antenna by 550 MHz [36]. In the same year, Christian et al. proposed a structural model of graphene conductivity regulation [37]. They analyzed the role of graphene in reconfigurable antennas at microwave frequency bands and designed two frequency-reconfigurable antennas, using copper as the body of the antenna and graphene as the switching structure of the antenna to provide reconfigurability of the antenna. The high-impedance state of graphene was simulated as a switched-off state, while the low-impedance mode was simulated as a switched-on state. One of the antennas was used for WI-FI systems with operating bands covering 2.4 GHz, 3.6 GHz, and 5 GHz, and the other antenna was used for LTE systems with operating bands including 1.7 GHz, 2.5 GHz, and 3.6 GHz. In 2022, Khatereh Moradi et al. used a metal ring as radiator, graphene film as rectangular strip, and two L-shaped elements in the central metal ring to change the chemical potential of graphene. The center frequency of the antenna could be adjusted between 3.82 THz and 5.93 THz [38].

In this paper, a frequency-reconfigurable microstrip patch antenna is designed according to the tunable conductivity property of graphene film. The antenna has a rectangular slot in its patch, and its slot is filled with graphene film. The frequency reconfigurability of the antenna is achieved by applying bias voltage to the graphene film. The bias voltage can adjust the conductivity of graphene and change the current distribution on the antenna's surface. Then, the frequency-reconfigurable antenna is fabricated and tested. The results show that the center frequency of the antenna was offset up to 10.4 GHz and that the antenna is well matched in both operating bands.

## 2. Experimental Methods

### 2.1. Preparation of Graphene Film

Monolayer graphene films were prepared via chemical meteorological deposition. Copper foil was placed in a CVD tube furnace (BTF-1200C, Beiyike Equipment Technology, Hefei, China) under a mixed atmosphere of 100 sccm (standard cubic centimeters per minute) of H<sub>2</sub> and 500 sccm Ar, and the temperature was increased to 1035 °C, while the air pressure inside the furnace was kept below 400 Pa. After reaching 1035 °C, 30 sccm of CH<sub>4</sub> was introduced as the carbon source to grow graphene films. After 15 min, the flow of CH<sub>4</sub> was stopped, and the copper foil was allowed to cool to room temperature under an atmosphere of 10 sccm H<sub>2</sub> and 500 sccm Ar. A schematic diagram of graphene growth via CVD can be seen in Figure S1.

The copper foil with a monolayer of graphene was spin-coated with PMMA solution (4% by mass), dried, and heated at 120 °C for 30 min. Subsequently, the copper foil was etched using ammonium persulfate solution (0.5 mol/L), and then the graphene with PMMA support layer was transferred to the copper foil with monolayer graphene film. Finally, stacked bilayer graphene film was obtained. A schematic diagram of the graphene transfer process can be seen in Figure S2.

### 2.2. Antenna Fabrication

The substrate of the antenna is a Si wafer with 10 nm of SiO<sub>2</sub>, and the metal layer is copper. The graphene film was firstly transferred to the Si wafer via PMMA wet transfer; then, the graphene film was processed using a laser-etching machine (SC-K600, Shengxiong Laser, Dongguan, China) to create a rectangle of 2 mm × 0.7 mm. Subsequently, a 1 μm thick copper sheet was vaporized on the surface using a vacuum coater (DZ-350, Chinese Academy of Sciences Shenyang Scientific Instruments, Shenyang, China); finally, the copper structure of the antenna was fabricated via UV lithography (ABM/6/350/NUV/DCCD/M, ABM, Silicon Valley, CA, USA).

### 2.3. Characterization and Testing

The prepared graphene films were characterized using Raman spectroscopy (Renishaw in Via Reflex, laser excitation energy of 532 nm, Renishaw, London, UK). The antennas were tested using a vector network analyzer (E5080B, Keysight Technologies, Santa Rosa, CA, USA).

## 3. Tunable Conductivity of Graphene Film

### 3.1. Graphene Film Characterization

The Raman spectra of graphene on the Si/SiO<sub>2</sub> substrate are presented in Figure 1. Figure 1a shows the Raman spectra of monolayer graphene. The intensity of the D peak located at the 1350 cm<sup>-1</sup> peak position is very weak, which indicates that the prepared CVD-grown monolayer graphene has fewer defects. The intensity of the 2D peak located at the peak position of 2700 cm<sup>-1</sup> is much larger than that of the G peak located at the 1580 cm<sup>-1</sup> peak position, and the ratio between them is about 2.6, which is a significant characteristic of the Raman spectrum curve of monolayer graphene [39]. This result proves that the prepared graphene is monolayer graphene. The Raman spectra of the stacked bilayer graphene are shown in Figure 1b. The characteristics of the Raman spectra of stacked bilayer graphene are almost the same as those of monolayer graphene [40]. The D peak intensity of stacked bilayer graphene is slightly increased, which may be explained by the fact that the stacking process may introduce impurities or cause graphene breakage.

The Raman spectrum results have demonstrated that the stacked bilayer graphene has the same Raman spectra characteristics as monolayer graphene, so Raman surface scanning was only applied to monolayer graphene. As can be seen in Figure 1c, the intensity ratio of the 2D and G peaks is larger than 2.25, which corresponds to monolayer graphene film. There are several small regions with smaller ratios, indicating that there are more graphene film layers in these regions than in the single layers, which is probably because this is the nucleation point during graphene's growth and the growth time is longer. From

Figure 1d, we observe that the intensity ratio of the D and G peaks is less than 0.25, and the entire surface is more uniform, indicating that the prepared monolayer graphene has fewer defects, is highly intact, and possesses good homogeneity.

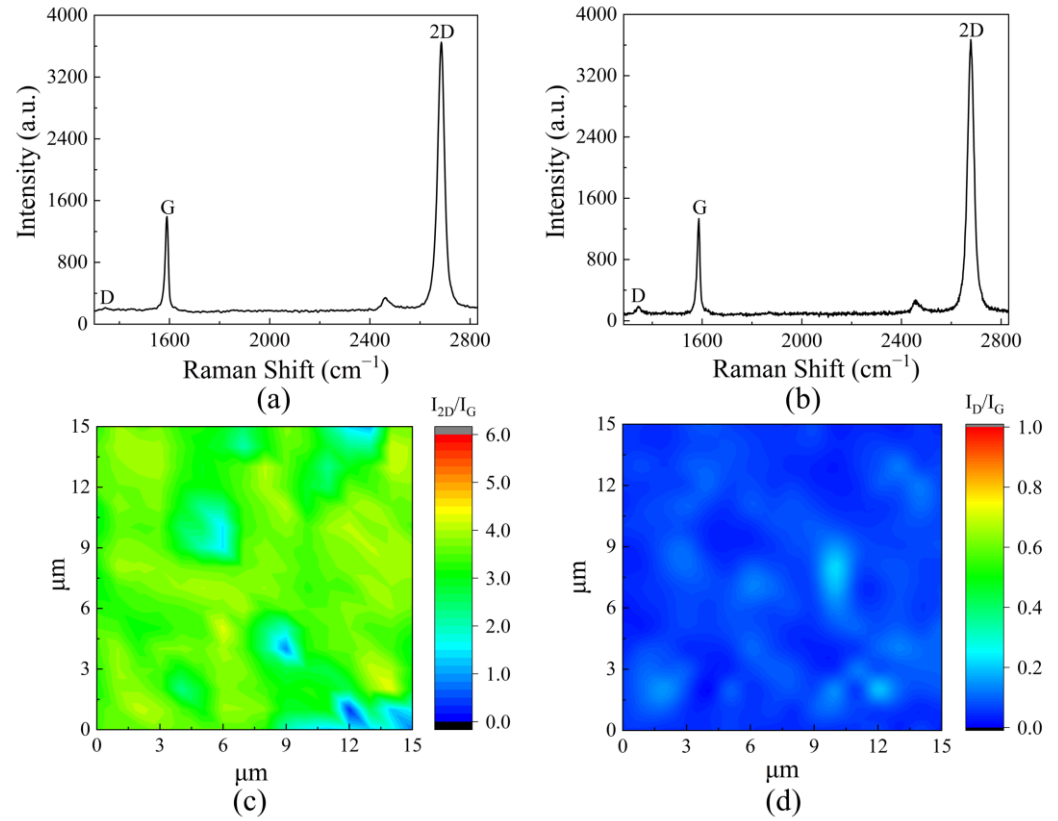


**Figure 1.** (a) Raman spectrum of monolayer graphene; (b) Raman spectrum of stacked bilayer graphene; (c) I<sub>2D</sub>/I<sub>G</sub> Raman surface scanning; (d) I<sub>D</sub>/I<sub>G</sub> Raman surface scanning.

### 3.2. Conductivity Model of Graphene Film

As a two-dimensional material, we can consider graphene as a thin film with complex surface conductivity, whose conductivity ( $\sigma_s$ ) can be calculated using the Kubo formula [41]:

$$\sigma_s(\omega, \mu_c, \Gamma_s, T) = \frac{-je^2 K_B T}{\pi \hbar^2 (\omega - 2j\Gamma_s)} \left\{ \frac{\mu_c}{K_B T} + 2 \ln \left[ \exp\left(-\frac{\mu_c}{K_B T}\right) + 1 \right] \right\} + \frac{je^2}{4\pi \hbar} \ln \left[ \frac{2|\mu_c| - (\omega - 2j\Gamma_s)\hbar}{2|\mu_c| - (\omega + 2j\Gamma_s)\hbar} \right] \quad (1)$$

where  $\omega$  is the angular frequency,  $\mu_c$  is the chemical potential of graphene,  $\Gamma_s$  is the carrier-scattering rate,  $T$  is the temperature in Kelvin,  $K_B$  is the Boltzmann constant,  $\hbar$  is the approximate Planck constant, and  $e$  is the electron charge constant, for which the scattering rate is inversely proportional to the relaxation time ( $\Gamma_s = 1/(2\tau)$ ). In Formula (1), the first term represents the intra-band conductivity of graphene, and the second term represents the inter-band conductivity of graphene. In the microwave and terahertz bands, the intra-band conductivity of graphene is the dominant form of graphene conductivity, while in the near-infrared and visible spectra, the inter-band conductivity plays a dominant role [42]. Therefore, the conductivity of graphene in the microwave and terahertz bands can be approximated by referencing the first term [43].

In addition, the chemical potential of graphene can be controlled by applying bias voltage [44]. The relationship between the bias voltage and the chemical potential of graphene is shown in Formula (2):

$$\mu_c = \hbar v_f \sqrt{\frac{\pi \epsilon_0 \epsilon_r}{e t_0} V_b} \quad (2)$$

where  $v_f$  is the Fermi velocity,  $t_0$  is the thickness of the dielectric layer between the graphene and the bias electrode,  $V_b$  is the magnitude of the bias voltage, and  $\epsilon_0$  and  $\epsilon_r$  are the vacuum dielectric constant and the dielectric layer dielectric constant, respectively. By employing  $T = 300$  K,  $\tau = 3$  ps,  $v_f = 10^6$  m/s, and  $t_0 = 10$  nm, the results of Figure 1 can be derived. Figure 2a shows the relationship between graphene's conductivity and chemical potential in the microwave band frequency. From the figure, it can be seen that both the real and imaginary parts of graphene conductivity increase with the increase in the chemical potential at the same frequency point, and the change in the real part is more significant than that of the imaginary part. The real part of the graphene conductivity at the same chemical potential does not vary much with the frequencies in the microwave band, and the imaginary part varies, but the value of the imaginary part is small and can thus be ignored. So, the conductivity of graphene in the microwave band can be approximated as a form of frequency-independent pure resistance, and the change in graphene conductivity due to frequencies can be ignored in the subsequent simulation. Figure 2b shows the graphene chemical potential versus bias voltage, which increases as the bias voltage rises [45,46]. Therefore, we can increase the conductivity of graphene by increasing the graphene bias voltage. In the microwave band, the change in the real part of the conductivity is mainly considered [47], while the change in the imaginary part is small and can thus be neglected.

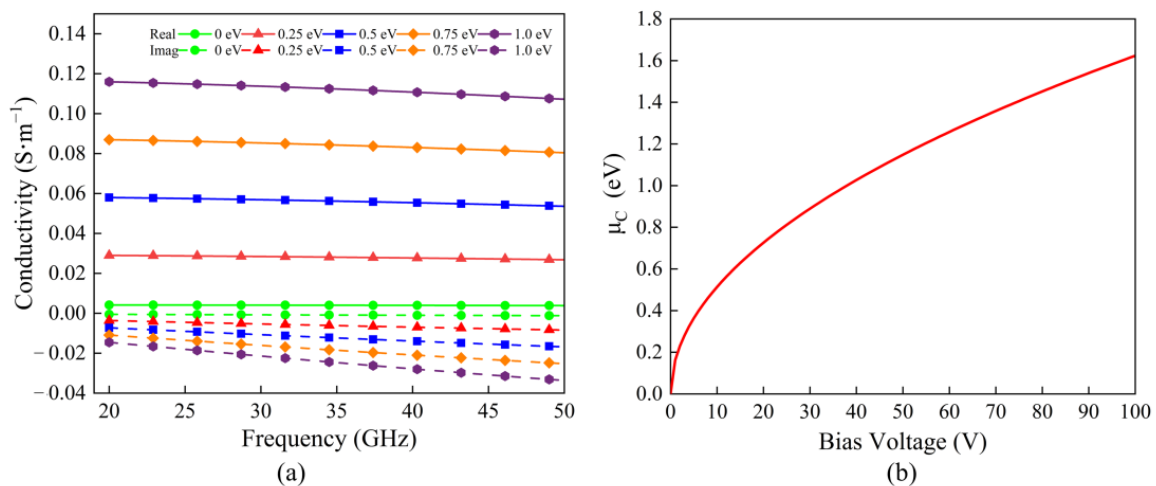


**Figure 2.** (a) Relationship curves between graphene conductivity and frequency at different chemical potentials; (b) relationship curves between graphene potential and bias voltage.

### 3.3. Adjustable Range Test Regarding Graphene Film's Square Resistance

The graphene films on the Si/SiO<sub>2</sub> substrate were used for the regulation of conductivity to explore the range of tunable conductivity. According to  $Z_s = 1/\sigma_s$ , the square resistance of graphene is inversely related to the conductivity of graphene, and the change of square resistance can reflect the change of conductivity under certain conditions. Therefore, the method of testing the square resistance of graphene is used in this study instead of testing the conductivity of graphene, and the square resistance of graphene can also be set as the input parameter in the subsequent simulation.

Figure 3a shows the experimental sample used to test the graphene resistance tuning range, showing the graphene film (presented in the dashed box), a silver paste (which was used as the electrode material), and a silicon wafer with an oxide layer thickness of 10 nm and a total thickness of 500  $\mu\text{m}$  (which was used as the substrate). The graphene is located in the middle of the silicon wafer and its size is 0.5 cm  $\times$  1 cm. There are three electrodes on both sides and in the middle of the graphene film. The electrodes on both sides are used to connect to the test equipment in order to test the square resistance of graphene, and the middle electrode is used to apply a bias voltage to regulate the square resistance of graphene. The test model of graphene's structure with adjustable conductivity is shown in Figure 3b, where a DC power supply is connected between the graphene and the silicon

wafer. The graphene film is connected to the positive pole of the power source, and the silicon substrate is connected to the negative pole of the power source. The conductivity of graphene is regulated by applying bias voltage. The square resistance of graphene is calculated using Ohm's law.

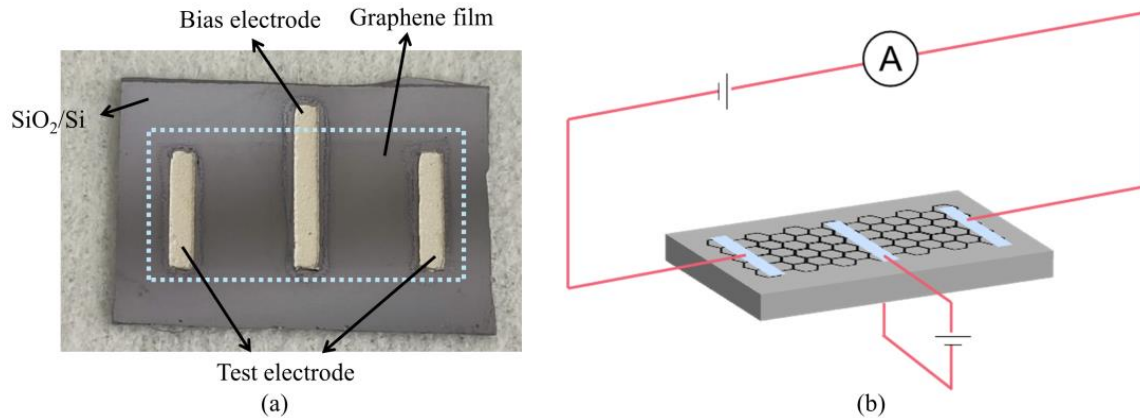


**Figure 3.** Graphene structure with adjustable conductivity. (a) Photograph of sample; (b) structure model.

Figure 4a shows that when the bias voltage is 0 V, the square resistance of the monolayer graphene film is  $1165 \Omega/\text{sq}$ . When the bias voltage is 5 V, the square resistance drops to  $445 \Omega/\text{sq}$ , amounting to a 61.8% decrease. Figure 4b shows the measured square resistance of the stacked bilayer graphene. When the bias voltage is 0 V, the square resistance of the stacked bilayer graphene film is  $416 \Omega/\text{sq}$ . When the bias voltage is 5 V, the square resistance decreases to  $208 \Omega/\text{sq}$ , which corresponds to a decrease of 50%. When the bias voltage reaches 10 V, the square resistance decreases to  $83 \Omega/\text{sq}$ , constituting a decrease of 80%. From the above test results, it can be seen that the monolayer graphene film is more sensitive to the applied bias voltage than the stacked bilayer graphene film. However, in the actual test, the oxide layer of the silicon wafer was broken down in both models when the bias voltage was too high, and the regulation effect of the square resistance was lost. The maximum bias voltage of the stacked bilayer graphene film is greater than that of the monolayer graphene film. Although the tunability of stacked bilayer graphene film is not as good as that of the monolayer graphene film, the actual tuning range of square resistance is larger than that of the monolayer graphene film.

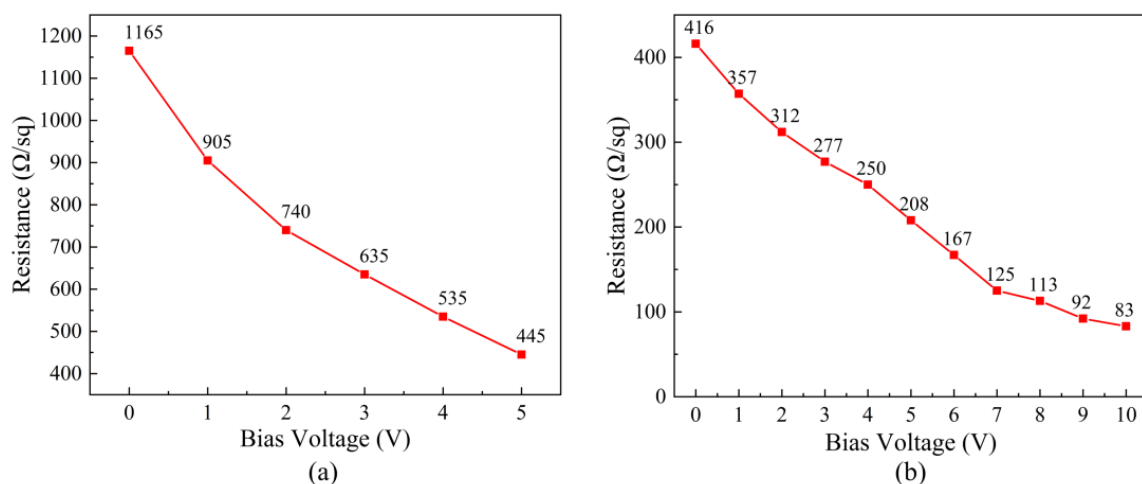


**Figure 4.** The resistance of graphene film vs. bias voltage. (a) Monolayer graphene; (b) bilayer graphene.

## 4. Frequency-Reconfigurable Antenna Based on Graphene Film

### 4.1. Antenna Structure Design

The schematic structure of the frequency-reconfigurable antenna based on graphene film is shown in Figure 5. The specific size parameters of the antenna are shown in Table 1. The antenna is composed of a slotted patch antenna and slot-filled graphene film. The graphene film is in direct contact with the Si/SiO<sub>2</sub> substrate, and copper is coated on the bottom of the substrate as the antenna's ground. An external DC power supply is used as the bias voltage. The graphene film connects to the positive pole of the power source, while the Si substrate connects to the negative pole of the power source. Adjusting the bias voltage changes the chemical potential of graphene, and the change in the chemical potential of graphene film will affect its surface impedance, while the change of graphene's impedance will induce a change in antenna surface current, thereby achieving the reconfigurability of antenna.

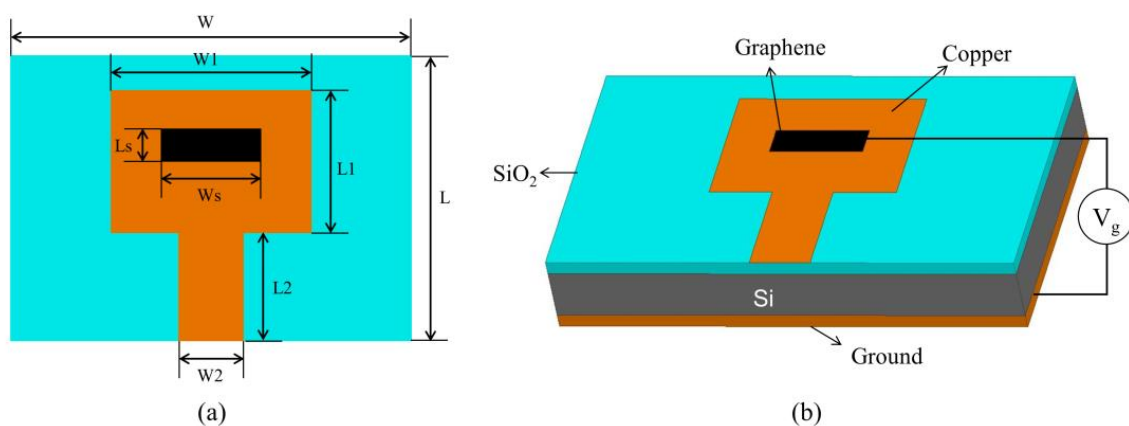


**Figure 5.** Antenna structure. (a) Front schematic; (b) overall schematic.

**Table 1.** Antenna size parameters.

Parameter	Value (mm)	Parameter	Value (mm)
W	10	L	6
W1	4	L1	3
W <sub>s</sub>	2	L <sub>s</sub>	0.7
W2	1.3	L2	2.27

### 4.2. Antenna Simulation Results

The designed antenna was simulated in HFSS (High Frequency Structure Simulator, Ansoft). Using the impedance boundary in HFSS, the graphene film was simulated as a pure resistor with fixed resistance. The adjustable range of square resistance of the two graphene films was used to simulate the graphene film. The parameters of the monolayer graphene film were set to 1100  $\Omega$ /sq and 500  $\Omega$ /sq to simulate the presence and absence of bias voltage, respectively, while the parameters of the stacked bilayer graphene film were set to 400  $\Omega$ /sq and 100  $\Omega$ /sq to simulate the presence and absence of bias voltage, respectively. The results of the simulated reflection coefficients are shown in Figure 6.

As shown in Figure 6, when the square resistance of graphene is 1100  $\Omega$ /sq and 500  $\Omega$ /sq, the center frequency of the antenna corresponds to 29.9 GHz and 30.3 GHz, and the change in frequency is only 0.4 GHz. When the square resistance of graphene is 400  $\Omega$ /sq and 100  $\Omega$ /sq, the center frequency of the antenna corresponds to 30.4 GHz and 39.1 GHz, and the change in frequency is 8.7 GHz. The simulation results indicate that the frequency-reconfigurable antenna using the stacked bilayer graphene film is more effective than the monolayer graphene film. Therefore, the stacked bilayer graphene films were used as the graphene component of the antenna in the subsequent experiments.

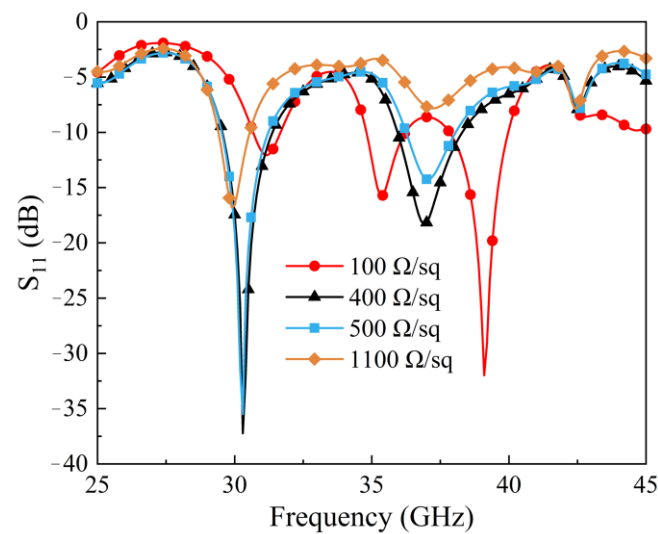


**Figure 6.** Simulation  $S_{11}$  of monolayer graphene and stacked bilayer graphene frequency-reconfigurable antenna.

Figure 7 shows the simulation results of the frequency-reconfigurable antenna incorporating stacked bilayer graphene. The simulation results of the antenna reflection coefficient are shown in Figure 7a; they show that the square resistance of graphene decreased from  $400 \Omega/\text{sq}$  to  $100 \Omega/\text{sq}$ , while the center frequency of the antenna increased from 30.4 GHz to 39.1 GHz, with a frequency change of 8.7 GHz. The corresponding reflection coefficients under the two operating bands are  $-39 \text{ dB}$  and  $-31.9 \text{ dB}$ , and the antenna is well matched. Figure 7b shows the radiation pattern of the antenna in the yoz plane at the two frequency bands. When the square resistance of the graphene film is  $400 \Omega/\text{sq}$ , the direction of the radiation of the antenna in the radiation pattern at 30.4 GHz is more dispersed and the gain is  $-0.4 \text{ dBi}$ , while when the square resistance of the graphene film is  $100 \Omega/\text{sq}$ , the direction of radiation of the antenna is more concentrated at 39.1 GHz and the gain is  $3.1 \text{ dBi}$ .

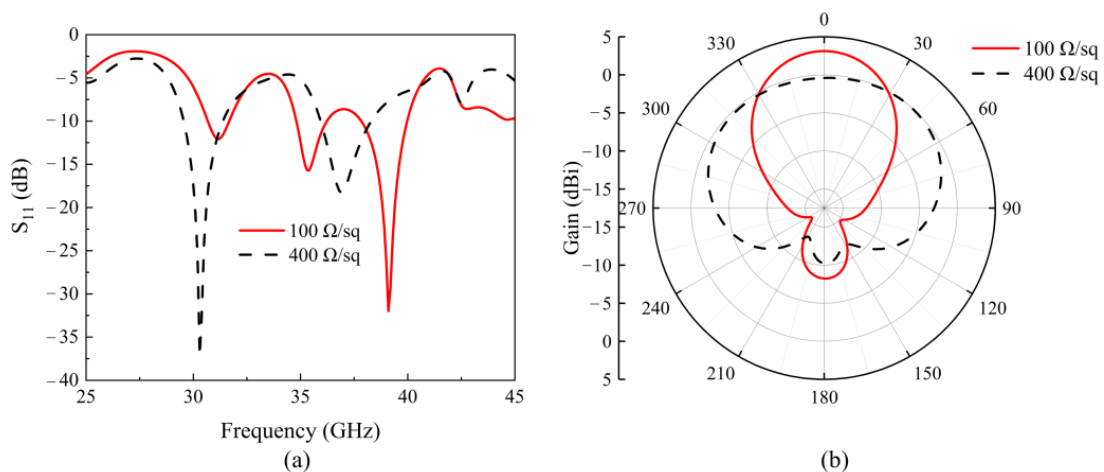


**Figure 7.** Simulation results of stacked bilayer graphene. (a)  $S_{11}$ ; (b) Yoz plane pattern.

The surface current distribution on the antenna patch under the two operating bands is shown in Figure 8. Figure 8a,b show the current distributions of the antenna at 30.4 GHz, and Figure 8c,d show the current distributions at 39.1 GHz. As shown in Figure 8a,b, when the square resistance of the graphene film is  $400 \Omega/\text{sq}$ , the current enters different phases, the surface current of the graphene part does not change greatly, and the current density is lower than that of the copper part. Since the square resistance of the graphene film is higher and its conductivity is lower, the current flows to a greater extent in the copper part of the antenna,

the graphene part does not influence the radiation of the antenna, and the radiation pattern of the antenna is close to the slotted patch antenna. The results in Figure 8c,d show that the phase of the current varies when the square resistance of the graphene film is 100 Ω/sq, and the surface current distribution of the graphene component is similar to the surrounding copper component. The surface current distribution changes with the phase change. The square resistance of the graphene film is low, and the corresponding conductivity is high, so the current flows uniformly in the copper and graphene components of the antenna. This result indicates that the graphene film is deeply involved in the radiation of the antenna and that the radiation pattern of the antenna is close to that of the patch antenna without slotting. The change in the square resistance of the graphene film leads to a change in the surface current distribution of the antenna at the two operating bands. The radiation mode of the antenna switches between the nearly slotted antenna and the nearly unslotted antenna, so the center frequency of the antenna also changes. Finally, the frequency reconfigurability of the antenna is realized. The variable radiation performance of the graphene component at the two operating bands is also the reason why the radiation direction map of the antenna is more concentrated when the graphene square resistance is 100 Ω/sq than when the graphene square resistance is 400 Ω/sq.

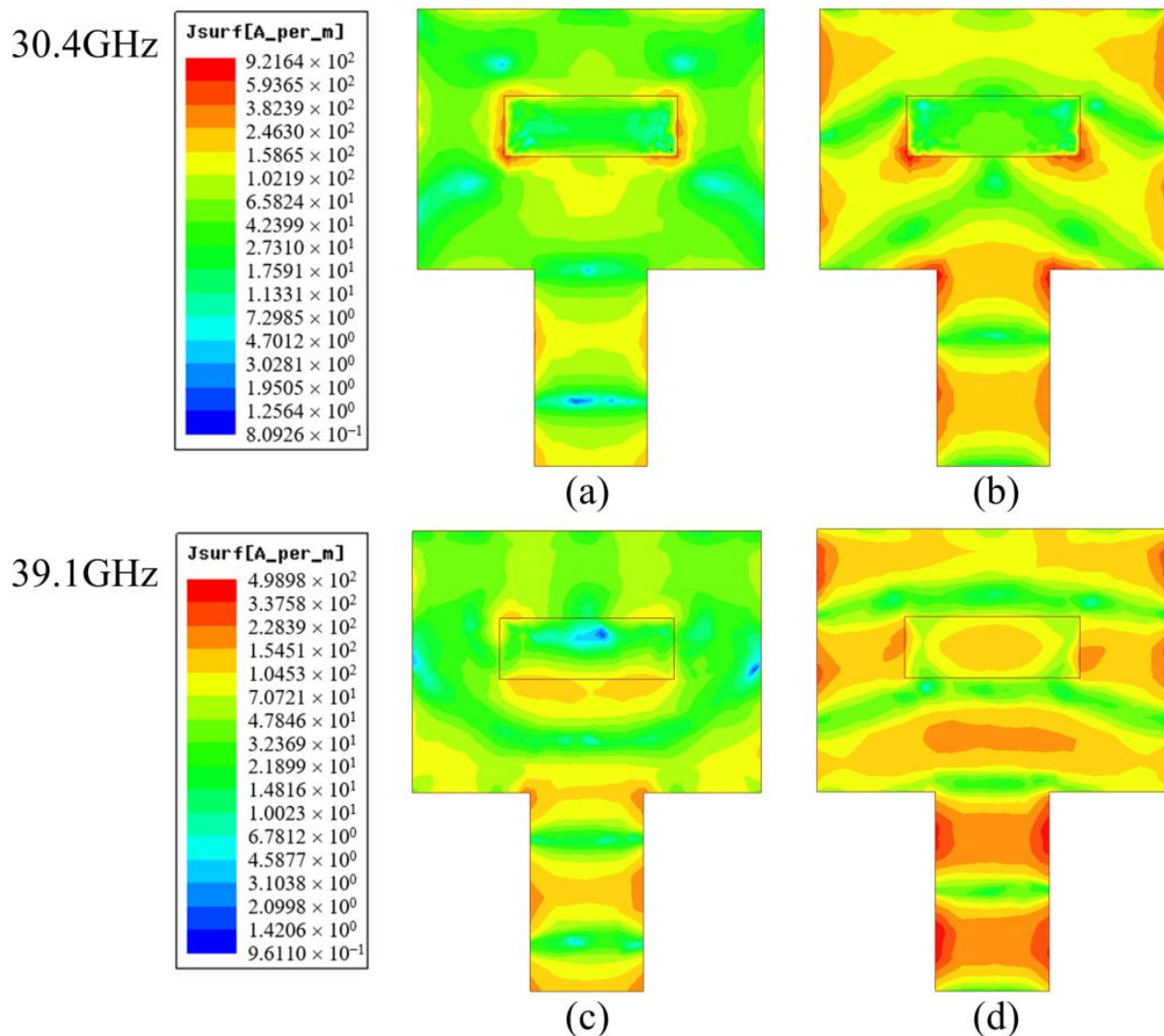
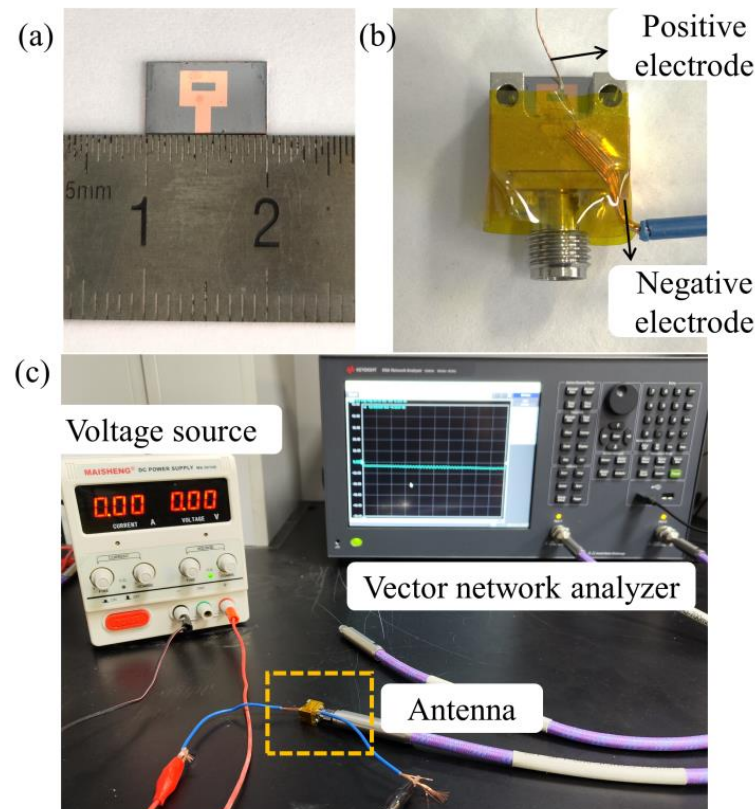


Figure 8. Surface current distribution of the frequency-reconfigurable antenna of the stacked bilayer graphene. (a) 400 Ω/sq, 0 deg; (b) 400 Ω/sq, 90 deg; (c) 100 Ω/sq, 0 deg; (d) 100 Ω/sq, 90 deg.

### 4.3. Antenna Performance

In order to verify the frequency reconfigurability of the designed antenna, an antenna prototype was fabricated, as shown in Figure 9a. Figure 9b shows the antenna with bias voltage. A DC voltage source was used to apply a bias voltage to the graphene film. The positive electrode of the power sources connects to the copper part of the antenna, and the negative electrode of the power sources connects to the housing of the connector. Bias voltage was applied to the ground plane of the antenna and the graphene film of the antenna patch according to the above connection method to change the graphene conductivity. The test environment of the antenna is shown in Figure 9c.



**Figure 9.** (a) Antenna prototype; (b) antenna prototype with bias voltage; (c) antenna measurement environment.

A comparison of the reflection coefficients between the measurement and simulation for the antenna is shown in Figure 10. The square resistance of the graphene film is  $400 \Omega/\text{sq}$  and  $100 \Omega/\text{sq}$  when applying a bias voltage of  $0 \text{ V}$  and  $9 \text{ V}$ , respectively. There are slight deviations between the simulated and tested results, but the overall trend of the curves remains consistent. When the bias voltage of  $0 \text{ V}$  is applied to the graphene, the center frequency of the antenna is  $29.6 \text{ GHz}$ , and the corresponding reflection coefficient is  $-26 \text{ dB}$ . When a bias voltage of  $9 \text{ V}$  is applied to the graphene, the center frequency of the antenna increases to  $40 \text{ GHz}$ , and the corresponding reflection coefficient is  $-20.8 \text{ dB}$ . Under the two bias voltages, the center frequency of the antenna is shifted by  $10.4 \text{ GHz}$ , and frequency reconfigurability is achieved. Thus, the frequency-reconfigurable function has been achieved, and the antenna is well matched at both bias voltages.

The antenna-measured and -simulated yoz-plane radiation patterns are shown in Figure 11. Figure 11a shows the simulated results of the antenna with  $400 \Omega/\text{sq}$  of graphene impedance at  $30.4 \text{ GHz}$  and the measured results of the antenna with  $0 \text{ V}$  bias voltage at  $29.6 \text{ GHz}$ . Figure 11b shows the simulated results of the antenna with  $100 \Omega/\text{sq}$  graphene impedance at  $39.1 \text{ GHz}$  and the measured results of the antenna with  $9 \text{ V}$  bias voltage at  $40 \text{ GHz}$ . It can be seen that the measured results basically match the simulated results: the

gain of the antenna at 29.6 GHz is  $-0.79$  dBi, and the efficiency of the antenna is 32% in this mode, while the gain of the antenna at 40 GHz is 2.7 dBi, and the efficiency of the antenna is 25% at this mode.

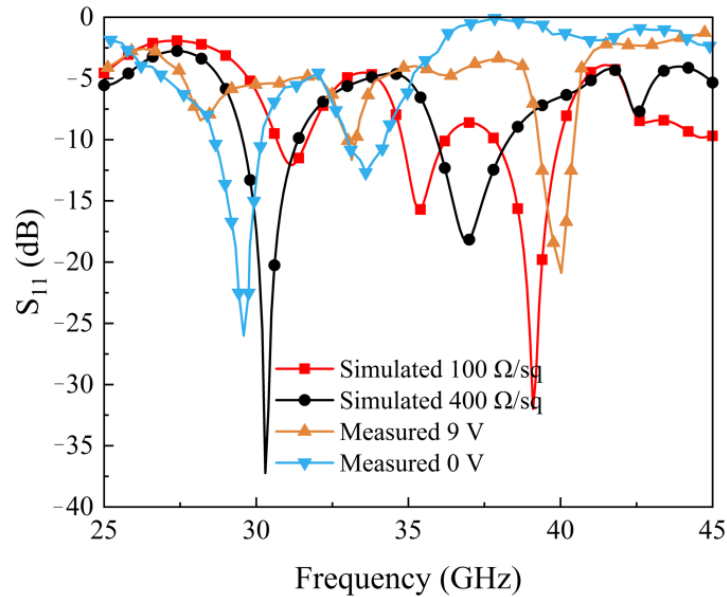


Figure 10.  $S_{11}$  of antenna measured and simulated.

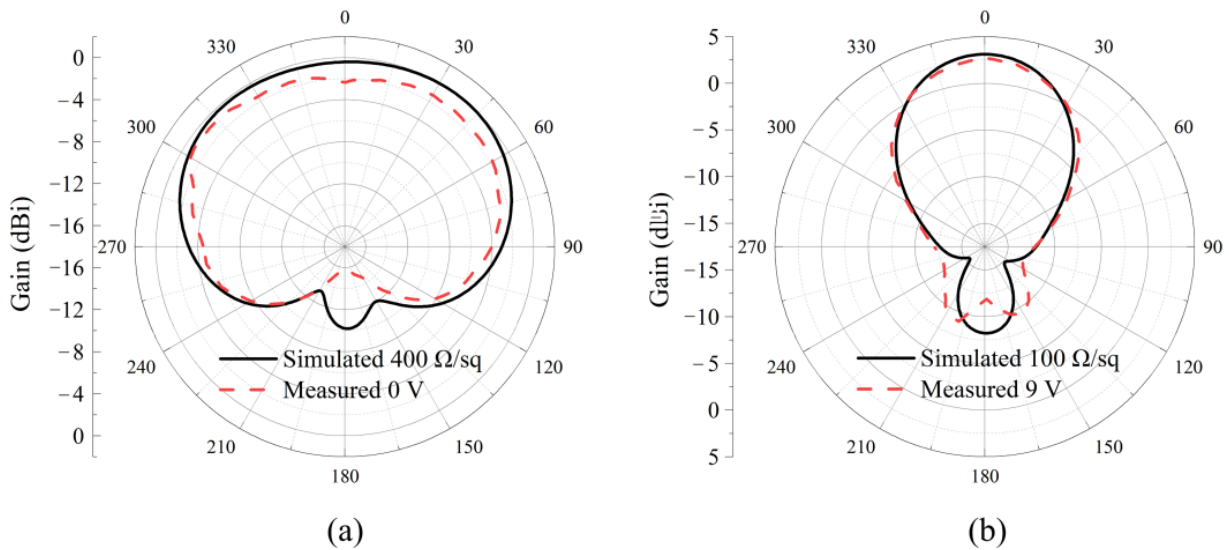


Figure 11. Antenna yoz-plane radiation patterns. (a) Simulated 400  $\Omega$ /sq vs. measured 0 V. (b) simulated 100  $\Omega$ /sq vs. measured 9 V.

Table 2 shows the performance of the antennas in this paper compared to antennas developed in previously published studies. These references utilize four methods to achieve antenna frequency reconfigurability. As can be seen from the table, the antenna in this paper achieves the maximum frequency shift. Compared to the antenna in reference [48], the antenna in this work is smaller despite operating at similar frequency bands. Although the antennas in reference [49] and reference [50] can be tuned to more operating bands by using two switches, this increases costs and design complexity. The bias voltage used in reference [34] is up to 200 V, while it was only 9 V in this work.

**Table 2.** Antenna performance comparison.

Ref.	Reconfigurable Method	Size (mm <sup>2</sup> )	Operation Frequency (GHz)	Frequency Shift (GHz)	Publication Years
[48]	Variable Capacitor	9.88 × 20.4	27.8, 28.8	1	2020
[49]	RF-MEMS	3 × 4.8	28, 29.2, 31.5, 35	7	2008
[50]	PIN	36.5 × 10	0.9, 2.0, 2.4	1.3	2015
[34]	Graphene	23 × 23	8.7, 11.3	2.6	2015
This work	Graphene	6 × 10	29.6, 40	10.4	

## 5. Conclusions

In summary, a frequency-reconfigurable microstrip patch antenna based on the tunable conductive properties of graphene has been proposed. High-quality monolayer graphene films were prepared using CVD and were stacked layer by layer to obtain stacked bilayer graphene films. The stacked bilayer graphene films were placed in the antenna radiation patch slot. The graphene's conductivity was changed by applying bias voltage to further change the surface current of the antenna. As a result, the operating mode of the antenna could be switched between a nearly slotted antenna and a nearly unslotted antenna to achieve frequency reconfigurability. The results of the square resistance adjustable range test conducted on graphene film show that the monolayer graphene film and stacked bilayer graphene film have square resistance adjustable ranges of 1165–445 Ω/sq and 416–83 Ω/sq, respectively. The HFSS simulation results show that the antenna incorporating the stacked bilayer graphene film has a larger center frequency adjustment range than the antenna incorporating the monolayer graphene film. To verify the frequency reconfigurability of the designed antenna, a prototype antenna was fabricated using stacked bilayer graphene film. The test results show that the center frequency of the antenna is 29.6 GHz when the bias voltage is 0 V and 40 GHz when the bias voltage is 9 V. The corresponding reflection coefficients are −26 dB and −20.8 dB, respectively.

**Supplementary Materials:** The following supporting information can be downloaded at: <https://www.mdpi.com/article/10.3390/electronics12102307/s1>, Figure S1: Schematic diagram of graphene growth by CVD; Figure S2: Schematic diagram of graphene transfer process; Figure S3: Antenna group delay; Figure S4: Antenna equivalent circuit model.

**Author Contributions:** Conceptualization, X.W., W.W. and L.W.; methodology, X.W. and W.W.; software, X.W. and H.C.; validation, X.W., L.W., H.C. and W.W.; formal analysis, X.W.; investigation, L.W. and W.W.; resources, W.W.; data curation, X.W. and W.W.; writing—original draft preparation, X.W.; writing—review and editing, L.W., H.C. and W.W.; visualization, W.W.; supervision, Z.L.; project administration, W.W. and Z.L.; funding acquisition, W.W. and Z.L. All authors have read and agreed to the published version of the manuscript.

**Funding:** This project was supported by the following foundation: National Key R&D Program Found of China (Grant No. 2021YFB3803002).

**Data Availability Statement:** All data that support the findings of this study are included within the article (and any Supplementary Files).

**Conflicts of Interest:** The authors declare no conflict of interest.

## References

1. Kamran Shereen, M.; Khattak, M.I.; Nebhen, J. A review of achieving frequency reconfiguration through switching in microstrip patch antennas for future 5G applications. *Alex. Eng. J.* **2022**, *61*, 29–40. [CrossRef]
2. Langer, J.C.; Zou, J.; Liu, C.; Bernhard, J.T. Micromachined reconfigurable out-of-plane microstrip patch antenna using plastic deformation magnetic actuation. *IEEE Microw. Wirel. Compon. Lett.* **2003**, *13*, 120–122. [CrossRef]
3. Haupt, R.L.; Lanagan, M. Reconfigurable Antennas. *IEEE Antennas Propag. Mag.* **2013**, *55*, 49–61. [CrossRef]
4. Tu, Y.; Al-Yasir, Y.I.A.; Ojaroudi Parchin, N.; Abdulkhaleq, A.M.; Abd-Alhameed, R.A. A Survey on Reconfigurable Microstrip Filter–Antenna Integration: Recent Developments and Challenges. *Electronics* **2020**, *9*, 1249. [CrossRef]

5. Ojaroudi, N.; Amiri, S.; Geran, F. Reconfigurable monopole antenna with controllable band-notched performance for UWB communications. In Proceedings of the 2012 20th Telecommunications Forum (TELFOR), Belgrade, Serbia, 20–22 November 2012; pp. 1176–1178.
6. Li, Y.; Li, W.; Ye, Q. A compact circular slot UWB antenna with multimode reconfigurable band-notched characteristics using resonator and switch techniques. *Microw. Opt. Technol. Lett.* **2014**, *56*, 570–574. [[CrossRef](#)]
7. Matthews, E.W.; Cuccia, C.L.; Rubin, M.D. Technology Considerations for the Use of Multiple Beam Antenna Systems in Communication Satellites. *IEEE Trans. Microw. Theory Tech.* **1979**, *27*, 998–1004. [[CrossRef](#)]
8. Ojaroudi Parchin, N.; Jahanbakhsh Basherlou, H.; Al-Yasir, Y.I.A.; Abdulkhaleq, A.M.; Abd-Alhameed, R.A. Reconfigurable Antennas: Switching Techniques—A Survey. *Electronics* **2020**, *9*, 336. [[CrossRef](#)]
9. Li, T.; Zhai, H.; Wang, X.; Li, L.; Liang, C. Frequency-Reconfigurable Bow-Tie Antenna for Bluetooth, WiMAX, and WLAN Applications. *IEEE Antennas Wirel. Propag. Lett.* **2015**, *14*, 171–174. [[CrossRef](#)]
10. Abutarboush, H.F.; Shamim, A. A Reconfigurable Inkjet-Printed Antenna on Paper Substrate for Wireless Applications. *IEEE Antennas Wirel. Propag. Lett.* **2018**, *17*, 1648–1651. [[CrossRef](#)]
11. Tawk, Y.; Costantine, J.; Christodoulou, C.G. A Varactor-Based Reconfigurable Filtenna. *IEEE Antennas Wirel. Propag. Lett.* **2012**, *11*, 716–719. [[CrossRef](#)]
12. Cetiner, B.A.; Jafarkhani, H.; Jiang-Yuan, Q.; Hui Jae, Y.; Grau, A.; Flaviis, F.D. Multifunctional reconfigurable MEMS integrated antennas for adaptive MIMO systems. *ICoM* **2004**, *42*, 62–70. [[CrossRef](#)]
13. Zohur, A.; Mopidevi, H.; Rodrigo, D.; Unlu, M.; Jofre, L.; Cetiner, B.A. RF MEMS Reconfigurable Two-Band Antenna. *IEEE Antennas Wirel. Propag. Lett.* **2013**, *12*, 72–75. [[CrossRef](#)]
14. Mahanta, P.; Anwar, F.; Coutu, R.A., Jr. Novel Test Fixture for Characterizing MEMS Switch Microcontact Reliability and Performance. *Sensors* **2019**, *19*, 579. [[CrossRef](#)]
15. Sugiura, S.; Iizuka, H. Reactively Steered Ring Antenna Array for Automotive Application. *IEEE Trans. Antennas Propag.* **2007**, *55*, 1902–1908. [[CrossRef](#)]
16. Singh, A.; Goode, I.; Saavedra, C.E. A Multistate Frequency Reconfigurable Monopole Antenna Using Fluidic Channels. *IEEE Antennas Wirel. Propag. Lett.* **2019**, *18*, 856–860. [[CrossRef](#)]
17. Li, C.; Xu, S.; Yang, F.; Li, M. Design and Optimization of a Mechanically Reconfigurable Reflectarray Antenna with Pixel Patch Elements Using Genetic Algorithm. In Proceedings of the 2019 IEEE MTT-S International Wireless Symposium (IWS), Guangzhou, China, 19–22 May 2019; pp. 1–3.
18. Costantine, J.; Tawk, Y.; Woodland, J.; Flaum, N.; Christodoulou, C. Reconfigurable antenna system with a movable ground plane for cognitive radio. *Microw. Antennas Propag. IET* **2014**, *8*, 858–863. [[CrossRef](#)]
19. Rocca, P.; Haupt, R. Dynamic Array Thinning for Adaptive Interference Cancellation. In Proceedings of the Fourth European Conference on Antennas and Propagation, Barcelona, Spain, 12–16 April 2010; pp. 1–3.
20. Tomasic, B.; Turtle, J.; Liu, S.; Schmier, R.; Bharj, S.; Oleski, P. The Geodesic Dome Phased Array Antenna for Satellite Control and Communication—Subarray Design, Development and Demonstration. In Proceedings of the IEEE International Symposium on Phased Array Systems and Technology, Boston, MA, USA, 14–17 October 2003; pp. 411–416.
21. Novoselov, K.S.; Geim, A.K.; Morozov, S.V.; Jiang, D.; Zhang, Y.; Dubonos, S.V.; Grigorieva, I.V.; Firsov, A.A. Electric Field Effect in Atomically Thin Carbon Films. *Science* **2004**, *306*, 666–669. [[CrossRef](#)]
22. Olabi, A.G.; Abdelkareem, M.A.; Wilberforce, T.; Sayed, E.T. Application of graphene in energy storage device—A review. *Renew. Sustain. Energy Rev.* **2021**, *135*, 110026. [[CrossRef](#)]
23. Mudusu, D.; Nandanapalli, K.R.; Lee, S.; Hahn, Y.-B. Recent advances in graphene monolayers growth and their biological applications: A review. *Adv. Colloid Interface Sci.* **2020**, *283*, 102225. [[CrossRef](#)]
24. Zhu, Y.; Murali, S.; Cai, W.; Li, X.; Suk, J.W.; Potts, J.R.; Ruoff, R.S. Graphene and graphene oxide: Synthesis, properties, and applications. *Adv. Mater.* **2010**, *22*, 3906–3924. [[CrossRef](#)]
25. Nguyen, K.T.; Zhao, Y. Integrated graphene/nanoparticle hybrids for biological and electronic applications. *Nanoscale* **2014**, *6*, 6245–6266. [[CrossRef](#)] [[PubMed](#)]
26. Gurunathan, S.; Kim, J.H. Synthesis, toxicity, biocompatibility, and biomedical applications of graphene and graphene-related materials. *Int. J. Nanomed.* **2016**, *11*, 1927–1945. [[CrossRef](#)] [[PubMed](#)]
27. Huang, Y.; Wu, L.S.; Tang, M.; Mao, J. Design of a Beam Reconfigurable THz Antenna With Graphene-Based Switchable High-Impedance Surface. *IEEE Trans. Nanotechnol.* **2012**, *11*, 836–842. [[CrossRef](#)]
28. Sherrott, M.C.; Hon, P.W.C.; Fountaine, K.T.; Garcia, J.C.; Ponti, S.M.; Brar, V.W.; Sweatlock, L.A.; Atwater, H.A. Experimental Demonstration of  $>230^\circ$  Phase Modulation in Gate-Tunable Graphene–Gold Reconfigurable Mid-Infrared Metasurfaces. *Nano Lett.* **2017**, *17*, 3027–3034. [[CrossRef](#)] [[PubMed](#)]
29. Wang, J.; Lu, W.B.; Liu, Z.G.; Zhang, A.Q.; Chen, H. Graphene-Based Microwave Antennas With Reconfigurable Pattern. *IEEE Trans. Antennas Propag.* **2020**, *68*, 2504–2510. [[CrossRef](#)]
30. Tamagnone, M.; Perruisseau-Carrier, J. Predicting Input Impedance and Efficiency of Graphene Reconfigurable Dipoles Using a Simple Circuit Model. *IEEE Antennas Wirel. Propag. Lett.* **2014**, *13*, 313–316. [[CrossRef](#)]
31. Grande, M.; Bianco, G.V.; Laneve, D.; Capezzuto, P.; Petruzzelli, V.; Scalora, M.; Prudenzeno, F.; Bruno, G.; D’Orazio, A. Gain and phase control in a graphene-loaded reconfigurable antenna. *Appl. Phys. Lett.* **2019**, *115*, 133103. [[CrossRef](#)]

32. Hanson, G.W. Dyadic Green's Functions for an Anisotropic, Non-Local Model of Biased Graphene. *IEEE Trans. Antennas Propag.* **2008**, *56*, 747–757. [[CrossRef](#)]
33. Gomez-Diaz, J.S.; Perruisseau-Carrier, J. Microwave to THz properties of graphene and potential antenna applications. In Proceedings of the 2012 International Symposium on Antennas and Propagation (ISAP), Nagoya, Japan, 29 October–2 November 2012; pp. 239–242.
34. Dragoman, M.; Neculoiu, D.; Bunea, A.-C.; Deligeorgis, G.; Aldrigo, M.; Vasilache, D.; Dinescu, A.; Konstantinidis, G.; Mencarelli, D.; Pierantoni, L.; et al. A tunable microwave slot antenna based on graphene. *Appl. Phys. Lett.* **2015**, *106*, 153101. [[CrossRef](#)]
35. Bunea, A.C.; Neculoiu, D.; Dragoman, M.; Konstantinidis, G.; Deligeorgis, G. X band tunable slot antenna with graphene patch. In Proceedings of the 2015 European Microwave Conference (EuMC), Paris, France, 7–10 September 2015; pp. 614–617.
36. Yasir, M.; Savi, P.; Bistarelli, S.; Cataldo, A.; Bozzi, M.; Perregrini, L.; Bellucci, S. A Planar Antenna with Voltage-Controlled Frequency Tuning Based on Few-Layer Graphene. *IEEE Antennas Wirel. Propag. Lett.* **2017**, *16*, 2380–2383. [[CrossRef](#)]
37. Álvarez, C.N.; Cheung, R.; Thompson, J.S. Performance Analysis of Hybrid Metal–Graphene Frequency Reconfigurable Antennas in the Microwave Regime. *IEEE Trans. Antennas Propag.* **2017**, *65*, 1558–1569. [[CrossRef](#)]
38. Moradi, K.; Pourziad, A.; Nikmehr, S. An efficient graphene-based reconfigurable terahertz ring antenna design. *AEU -Int. J. Electron. Commun.* **2022**, *149*, 154177. [[CrossRef](#)]
39. Ferrari, A.C.; Meyer, J.C.; Scardaci, V.; Casiraghi, C.; Lazzeri, M.; Mauri, F.; Piscanec, S.; Jiang, D.; Novoselov, K.S.; Roth, S.; et al. Raman Spectrum of Graphene and Graphene Layers. *Phys. Rev. Lett.* **2006**, *97*, 187401. [[CrossRef](#)]
40. Bae, S.; Kim, H.; Lee, Y.; Xu, X.; Park, J.-S.; Zheng, Y.; Balakrishnan, J.; Lei, T.; Ri Kim, H.; Song, Y.L.; et al. Roll-to-roll production of 30-inch graphene films for transparent electrodes. *Nat. Nanotechnol.* **2010**, *5*, 574–578. [[CrossRef](#)] [[PubMed](#)]
41. Hanson, G.W. Dyadic Green's functions and guided surface waves for a surface conductivity model of graphene. *J. Appl. Phys.* **2008**, *103*, 064302. [[CrossRef](#)]
42. Dash, S.; Patnaik, A. Behavior of graphene based planar antenna at microwave and terahertz frequency. *Photonics Nanostruct.–Fundam. Appl.* **2020**, *40*, 100800. [[CrossRef](#)]
43. Zhang, Y.; Li, T.; Zeng, B.; Zhang, H.; Lv, H.; Huang, X.; Zhang, W.; Azad, A.K. A graphene based tunable terahertz sensor with double Fano resonances. *Nanoscale* **2015**, *7*, 12682–12688. [[CrossRef](#)]
44. Wang, X.C.; Zhao, W.S.; Hu, J.; Yin, W.Y. Reconfigurable Terahertz Leaky-Wave Antenna Using Graphene-Based High-Impedance Surface. *IEEE Trans. Nanotechnol.* **2015**, *14*, 62–69. [[CrossRef](#)]
45. Kushwaha, R.K.; Karuppanan, P. Proximity-coupled high gain graphene patch antenna using holey dielectric superstrate for terahertz applications. *Optik* **2021**, *240*, 166793. [[CrossRef](#)]
46. Li, J.; He, M.; Wu, C.; Zhang, C. Radiation-Pattern-Reconfigurable Graphene Leaky-Wave Antenna at Terahertz Band Based on Dielectric Grating Structure. *IEEE Antennas Wirel. Propag. Lett.* **2017**, *16*, 1771–1775. [[CrossRef](#)]
47. Perruisseau-Carrier, J.; Tamagnone, M.; Gomez-Diaz, J.S.; Carrasco, E. Graphene antennas: Can integration and reconfigurability compensate for the loss? In Proceedings of the 2013 European Microwave Conference, Nuremberg, Germany, 6–10 October 2013; pp. 369–372.
48. Choi, J.; Park, J.; Youn, Y.; Hwang, W.; Seong, H.; Whang, Y.N.; Hong, W. Frequency-Adjustable Planar Folded Slot Antenna Using Fully Integrated Multithrow Function for 5G Mobile Devices at Millimeter-Wave Spectrum. *IEEE Trans. Microw. Theory Tech.* **2020**, *68*, 1872–1881. [[CrossRef](#)]
49. Van Caekenberghe, K.; Sarabandi, K. A 2-Bit Ka-Band RF MEMS Frequency Tunable Slot Antenna. *IEEE Antennas Wirel. Propag. Lett.* **2008**, *7*, 179–182. [[CrossRef](#)]
50. Lee, S.W.; Sung, Y. Compact Frequency Reconfigurable Antenna for LTE/WWAN Mobile Handset Applications. *IEEE Trans. Antennas Propag.* **2015**, *63*, 4572–4577. [[CrossRef](#)]

**Disclaimer/Publisher's Note:** The statements, opinions and data contained in all publications are solely those of the individual author(s) and contributor(s) and not of MDPI and/or the editor(s). MDPI and/or the editor(s) disclaim responsibility for any injury to people or property resulting from any ideas, methods, instructions or products referred to in the content.